Microwave detected, microwave-optical double resonance of NH_3, NH_2D, NHD_2, and ND_3: I. Structure and force field of the $\tilde{A}$ state.*

Steven A. Henck,† Martin A. Mason, Wen - Bin Yan,‡ and Kevin K. Lehmann
Department of Chemistry, Princeton University, Princeton, NJ 08544

and Stephen L. Coy
Harrison Regional Spectroscopy Laboratory, Massachusetts Institute of Technology, Cambridge, MA 02139

Abstract

Microwave detected, microwave-optical double resonance was used to record the $\tilde{A}$ state electronic spectrum of NH_3, NH_2D, and NHD_2 with both vibrational and rotational resolution. To investigate ND_3 with the same resolution as we had with our hydrogen containing isotopomers, a strip-line cell was constructed allowing the simultaneous passage of radio-frequency and ultraviolet radiation. Rotational constants were obtained as a function of ν_2 excitation and an $\tilde{A}$ state equilibrium bond length was estimated at 1.055(8) Å. In addition, the harmonic force field for the $\tilde{A}$ state has been experimentally determined. f_{hh}, $f_{\alpha\alpha} - f_{\alpha\alpha'}$, and f_{rr} were found to be 1.06(4) aJ/Å^2, 0.25(2) aJ, and 4.9 aJ/Å^2 respectively. This calculated harmonic force field predicts that the asymmetry observed in the NH_3 2^4 band is due to a strong anharmonic interaction with the 4^3 level and the broad feature observed in the dispersed fluorescence spectrum previously assigned to the 1^1 band is more likely attributable to the 4^2 level.

*This work is taken in part from the Ph. D. thesis of Steven A. Henck.[1]

†Present address: Texas Instruments, 13536 N. Central Expy., MS 992, Dallas, TX 75243

‡Present address: Energia, Inc., P. O. Box 1468, Princeton, NJ 08542

I. INTRODUCTION

The lowest excited singlet state of ammonia, the $\tilde{A}$ state, has been subject to extensive spectroscopic study by a range of methods. However, since the first report by Leifson [2], it has been known that conventional techniques provide a limited amount of information. Leifson reported that the $\tilde{A}$ state absorption begins at about 220 nm, principally consists of a single long progression, and is diffuse. He interpreted this diffuseness as due to a rapid predissociation of the excited state such that the one photon spectrum shows resolved vibrational but not rotational structure. Walsh and Warshop [3] were able to show that the excited state is planar; hence, the long progression observed by Leifson [2] resulted from a large displacement of ν_2, the out-of-plane bending mode. They also showed that the $\tilde{A}$ state has A_2'' electronic symmetry and an N–H bond length greater than that of the ground electronic state.

With higher resolution than previous investigations, Douglas [4] partially resolved the rotational structure in the two lowest vibronic bands of ND_3 and obtained rotational constants for these levels. Analysis of the rotational constants neglecting vibration-rotation interactions confirmed the prediction of Walsh and Warshop [3] suggesting that in the excited state, the N–D bond length was significantly displaced. Such a large displacement in this coordinate also implied that in the absorption spectrum, a second progression in the symmetric stretching mode should also have been observed. As expected from above, a long progression in ν_1 is observed in the $\tilde{A}$ state resonance Raman spectrum [5] and dispersed emission from the ND_3 2^1 level [6].

Several hypotheses have been given to explain how the ν_1 progression is missing in absorption but seen in emission. As initially suggested by Harshbarger [7], one hypothesis proposes that the separate ν_1 progression was not observed in absorption because the ν_2 and ν_1 modes were in a near 3:1 degeneracy, the separate ν_1 progression being buried underneath the more intense ν_2 progression. However, even under the cold conditions of a jet expansion, no separate progression was revealed for NH_3 or ND_3 [8]. Another one proposes that the ν_1 mode predissociates so rapidly that its broad transition width precludes its observation [9]. Ashfold *et al.* [10] have observed a feature that they assigned to the ν_1 fundamental in dispersed fluorescence from the higher lying $\tilde{C}'$ state. They reported transition widths of 500 cm^{-1} for these bands. In the following paper [11], we will examine the predissociation of the $\tilde{A}$ state in detail. On the basis of that work, we assign the barrier to N-H dissociation as 2075 cm^{-1}, implying essentially direct dissociation from levels with the N–H stretching mode excited. As a result, we believe that any ν_1 progression would produce an essentially continuous absorption. Tang *et al.* [12] provided a third explanation for the lack of a ν_1 progression in the absorption spectrum. Using a model surface, with a small change in bond length at the ground state minimum, but a large change near the excited state planar geometry, they calculate that there should be ν_1 activity in emission but not absorption from the ground state. Thus, the two need not have the 'symmetry' that is predicted by normal mode theory.

The $\tilde{A} \leftarrow \tilde{X}$ transition has also been thoroughly investigated by a variety of theoretical techniques. From the CASSCF and CEPA wavefunctions for the symmetric modes, Rosmus *et al.* [13] calculated the potential energy surfaces (PES) for both the $\tilde{X}$ and $\tilde{A}$ states. These calculations confirmed that the $\tilde{A} \leftarrow \tilde{X}$ transition was accompanied by a planar $\leftarrow$ pyramidal

geometry change and that the N-H(D) equilibrium bond length is longer in the excited state; yet, the calculated $\tilde{A}$ state N– H(D)bond length was still much less than the experimental estimate [3,4,7]. They proposed that this discrepancy was due to errors caused by neglect of vibration-rotation interactions in reducing the observed rotational constants to an equilibrium geometry. The smaller displacement in this coordinate reduces the expected intensity of the missing ν_1 progression compared to the previous estimates [7].

Imre and co-workers [9,12,14] have modeled the $\tilde{A} \leftarrow \tilde{X}$ absorption spectrum using a time-dependent formalism. Using the unmodified potential of Rosmus *et al.* [13] with only the out-of-plane bend and symmetric stretching coordinates modeled, their calculated spectrum peaks to the red of the observed one. Agreement between experimental and calculated spectra was only achieved by modifying the potential of Rosmus *et al.* [13] to include a longer N-H bond length. However, increasing the N-H bond length also increases the ν_1 Franck-Condon factors. Hence, a progression in ν_1 is again predicted. In their work [12], however, they found that ν_1 and $3\nu_2$ progressions moved in a concerted fashion to yield in absorption only a single progression. Because of their neglect of the asymmetric stretching modes, their calculation did not include the effects of predissociation to NH_2 and H, and therefore, the lifetime broadening of these levels.

Rosmus *et al.* [13] calculated the ν_1 frequency at 2835 cm^{-1}. However, through dispersed fluorescence from the longer lived $\tilde{C}'$ state [15], the frequency of this mode was measured at 2300 ± 500 cm^{-1} [10]. Dixon [16] resolved this discrepancy by including in the theoretical determination interactions between ν_1 and the dissociative ν_3 coordinate. Inclusion of these interactions also enabled Dixon to accurately model the observed transition widths [16]. However, unlike the previous reports [7,9], a 1:3 degeneracy between ν_1 and ν_2 was not supported.

Utilizing the longer lifetime of the $\tilde{C}'$ state [15], the $\tilde{A}$ state has been studied by optical-optical double resonance techniques (OODR) [10,17]. These techniques simplify the spectrum by being sensitive to changes in only a single rovibrational level at a time. In the OODR method, rovibrational selectivity is accomplished by laser multiphoton excitation of a specific J_K line in the $\tilde{C}'$ state. Xie and coworkers [17], who were the first to apply this method to $\tilde{A}$ state ammonia, used a second tunable laser to ionize ammonia. When this second laser was in resonance with a downward $\tilde{C}' \rightarrow \tilde{A}$ transition from the initially populated level, the ionization signal was depleted. They reported the NH_3 $\tilde{A}$ state 2^0, 2^1, and 2^2 bands with both J and K resolution. They determined the B and C rotational constants for these levels to 0.3-0.03 cm^{-1} accuracy. Interestingly, these constants agree within experimental error with previous estimates from line shape analysis [18]. Later, Ashfold *et al.* [10] performed a similar experiment except with fluorescence-dip detection. They used much lower dump laser power and observed a significant decrease in transition widths demonstrating that the results of Xie *et al.* [17] suffered from significant power broadening.

Microwave detected, microwave-optical double resonance (MODR) has been used to investigate the vibrational overtones of ammonia in the visible region [19]. As the OODR techniques previously described, this technique allows one to measure the absorption spectrum of a single rovibrational level at a time. The principal advantage of this method is that selectivity is based upon the well-known ground state microwave spectrum [20–22]. In contrast, the OODR technique uses the less characterized $\tilde{C}'$ state transitions [15]. Furthermore, predissociation in the $\tilde{C}'$ state limits the range of $\tilde{A}$ state rovibronic levels that can

be reached. Since the ground state microwave transitions are known for all ammonia isotopomers [23–25], the MODR method can be relatively easily extended to the investigation of the entire isotopomeric series. Following the completion of this work, Endo and coworkers [26] reported the use of this technique to the study of the 2^1 level of the NH_3 $\tilde{A}$ state. They reported the homogeneous linewidths and positions of nearly fifty transitions to this band. Our work, even though not as extensive as theirs for this level, confirms their findings. We have extended this technique to the study of the higher NH_3 $\tilde{A}$ state vibronic levels. In addition, we have applied this technique to the study of the isotopomers NH_2D, NHD_2, and ND_3.

In ND_3, the inversion frequency drops to less than 2 GHz [23,25] so that for the investigation of this isotopomer, the identical spectrometer could not be used. In order to investigate the double resonance spectrum of this isotopomer, we constructed a radio-frequency detected, radio-frequency optical double resonance spectrometer (RFODR) similar to the MODR spectrometer. The principal difference between the two instruments was that in the RFODR spectrometer, the waveguide cell was replaced by a strip-line cell that simultaneously allowed the passage of radio-frequency and ultraviolet radiation. Using this cell, we were able to record the rovibrational contours of the 2^0, 2^1, and 2^2 bands of the ND_3 $\tilde{A}$ state with the same sensitivity that we had with the other isotopomers.

In this paper, we report on the $\tilde{A}$ transition frequencies we have observed by MODR and RFODR for the entire isotopomeric series. This experiment represents the most extensive spectroscopic investigation of the $\tilde{A}$ state of ammonia conducted to date. The goals of this study were the following. First, using the RFODR spectrometer, the resolution in the ND_3 2^1 spectrum was increased such that the centrifugal distortion coefficients for this level were derived. Second, for all isotopomers, precise rotational constants and vibrational term values were derived as a function of ν_2. From this data set, the harmonic force field of the $\tilde{A}$ state was determined. This newly derived force field leads us to reassign the broad features observed by Ashfold *et al.* [15] in dispersed fluorescence from the $\tilde{C}'$ state as due to ν_4 instead of ν_1. Third, with the more extensive rotational data, the vibration-rotation interaction term values were estimated allowing corrections to be obtained for the experimentally determined N-H(D) equilibrium bond length. This newly derived experimental estimate for r_e is in excellent agreement with the *ab initio* prediction of Rosmus *et al.* [13]. And lastly, these MODR experiments have allowed us to more accurately model the rotational and vibrational dependence of the transition widths. This topic will be addressed in the following paper [11].

II. EXPERIMENTAL

A schematic of the MODR spectrometer is shown in figure 1. This apparatus is similar to that used by Coy and Lehmann [19] except that ours does not include a microwave bridge to null the detector. The bridge increased signal to noise in the earlier work since it allowed for the use of greater ammonia pressure. In the current experiment, ammonia pressure was limited by the strong absorption cross section of the $\tilde{A} \leftarrow \tilde{X}$ transition and the need to keep the sample optically thin so as not to distort the observed lineshapes. The pulsed optical radiation was provided by a XeCl excimer pumped dye laser (Questek 2420/ Lambda Physik 3002E, respectively) using one of the following two schemes. To generate radiation from 207

nm to 220 nm, output from the dye laser using stilbene 3 (Exciton) as a gain medium was frequency-doubled in a β-BBO (Skytek) cut at 80°; or, to generate radiation from 197 to 210 nm, the output of rhodamine B (Lambda Physik) was tripled. Tripling was accomplished by first doubling in a KDP crystal using an Inrad Autotracker II. The remaining fundamental and second harmonic (300 nm) output of the KDP crystal are orthogonally polarized. To rotate the two beams such that they are parallel polarized, they are both passed through a 600 nm 0-order half-wave plate that acts as an approximate full waveplate for the second harmonic. The resulting nearly parallel polarized beams are then sum frequency mixed in the type 1 β-BBO crystal. Typical ultraviolet power was 50-100 μJ per pulse.

In the MODR experiments, continuous-wave microwave radiation was provided by a series of Oki klystrons phaselocked at selected ground state inversion frequencies. A two meter long WR-42 ("P" band) waveguide cell was used. At each end of the cell, a $0.020''$ (0.51 mm) thick sapphire window and a specially machined E-plane bend were mounted. These bends had a $1/8''$ hole drilled at the zero current line to allow ultraviolet radiation to enter and leave the cell, while the microwave radiation turned the corner. The cell was internally gold-plated to significantly reduce ammonia adsorption. The microwave power transmitted through the cell was detected by a Schottky-barrier detector diode and recorded by gated boxcar integrator triggered by the pulsed laser. The ultraviolet and microwave radiation had parallel polarizations. Since the microwave probes were Q branch rotation-inversion transitions, polarization effects enhance Q branch transitions, and weaken P and R branch transitions compared to the Hönl-London line strength factors applicable to absorption from an isotropic sample.

NH_3(Matheson, 99.995%) and ND_3 (Cambridge Isotopes, 99.5%) were used after purification through several freeze pump thaw cycles. The gas samples were flowed continuously through the cell at a set pressure to avoid depletion of the observed signals caused by photodecomposition. The mixed isotopes were prepared by combining NH_3 and ND_3 in the ratios 1:2 and 2:1 to maximize the ratio of NHD_2 and NH_2D, respectively. That the gas samples consisted of a mixture of isotopomers was not a problem since a transition between a single ground state inversion level of a particular isotopomer was selected and monitored by the microwave radiation. In all experiments, optimal signals were obtained at pressures between 10 and 70 mtorr.

Scanning and calibration of the laser were achieved by conventional methods [27]. Briefly, the transmission of an etalon and the optogalvanic signal from a Fe/Ne [28] hollow cathode lamp or the absorption of a $^{131}Te_2$ cell [29] were recorded for relative and absolute frequency calibration. The ultraviolet power was monitored for both signal normalization, and for computer control of the β-BBO crystal phase matching angle. At the same time, the detected microwave signal was amplified and sent to a gated boxcar integrator. These four signals were recorded by an IBM AT that also stepped the dye laser and maximized the ultraviolet conversion.

When the ultraviolet frequency coincided with a $\tilde{A} \leftarrow \tilde{X}$ transition, the optical pulse created a transient population difference between ground state inversion levels. The microwave signal is absorptive if the upper state is dpleted by the optical pulse, and emissive if the lower state is depleted. This is determined by the selectrion rules for the $\tilde{A} \leftarrow \tilde{X}$ transition. These rules are that symmetric inversion levels have allowed transitions to even number of quanta in ν_2 while anti-symmetric inversion levels have allowed transitions to odd number

of quanta in ν_2. Hence, the detected microwave intensity initially increased or decreased depending whether the final ν_2 quantum number was even or odd, respectively. A typical double resonance signal is shown in figure 2. Since this signal was observed through the excitation to the NH_2D 2^0 level, the microwave intensity initially increased. Phase sensitivity was achieved by setting a boxcar gate over the first hump of this Rabi nutation.

A representative MODR scan is shown in figure 3. The locked microwave frequency was resonant with the NH_3 $J_K = 6_6$ inversion doublet as the optical radiation was scanned. When the ultraviolet frequency was in resonance with the 6_6 line of the $\tilde{A}$ $2^3 \leftarrow \tilde{X}$ 2^0 band, the upper component of the inversion doublet was depleted and a decrease in microwave intensity detected. Further to the blue when the ultraviolet frequency came into resonance with the 6_6 line of the $\tilde{A}$ $2^4 \leftarrow \tilde{X}$ 2^0 band, the lower component of the inversion doublet was depleted and an increase in microwave intensity was detected. For this particular scan, only the Q branches were observed due to the parallel polarization of the two fields and the Hönl-London factors, both of which enhance the Q over the R branch transition in this case.

The inversion transitions in ND_3 are near 1.6 GHz [23,25], well below the cut off frequency of our MODR cell. While in principle, one could build a cell using much larger waveguide, this would necessarily lead to a very poor overlap of the microwave radiation with the ultraviolet pumped molecules. Instead, we constructed a RFODR cell based upon a strip-line cell. A cross section of the strip-line cell is shown in figure 4. The main components of the cell are a $5 \times 5 \times 200$ cm aluminum outer body, a $0.8 \times 0.8 \times 200$ cm aluminum center conductor, an aluminum ground plane, and two S1-UV windows mounted on flanges at each end of the cell. The center conductor was held at a fixed distance from the ground plane by KEL-F blocks. Originally, the distance (2 mm) was chosen to reduce radio-frequency reflections by impedance matching the cell to the source and detector impedance. However, with this spacing, beam divergence and scattering of the ultraviolet light produced a large photoelectron signal from the aluminum strip and ground plane that prevented detection of any double resonance signal. By placing rf hi-pass filters at each end of the cell, adding approximately 100 mtorr SF_6 that acted as an electron scavenger, and doubling the spacing between the center conductor and the ground plane, the anomalous photoelectron signal was reduced to a manageable level. No increase in noise level due to impedance mismatch was noticed. Radiation for the RFODR spectrometer was produced by a General Radio 1218-A unit oscillator. The rf power was measured by a HP 8473B crystal detector while all other features of the spectrometer are identical to the MODR setup previously described.

As will be discussed below, the lifetime for predissociation from the lowest levels of ND_3 is much longer than those of the other isotopomers. As a result, as first shown by Douglas [4], one observes partial rotational structure even in absorption. The double resonance data was dominated by high K transitions since the intensity of the radio-frequency probe transition scales as $(K/J(J+1))^2$. A fluorescence excitation spectrum of the ND_3 $\tilde{A}$ state 2^1 band was taken since the P and R branches have the highest Hönl-London factors for the low K levels. The pulsed laser system described in the double resonance experiments was used as the excitation source. Calibration was achieved in an identical fashion. The output was passed through a 34 cm long, heavily baffled cell in which ND_3 was slowly flowed to maintain a pressure of 0.5 torr. Fluorescence was detected at right angles to the laser propagation direction with an EMI 9635QB photomultiplier and boxcar detected. The resulting spectrum is shown in figure 5.

III. DATA ANALYSIS

The observed peaks were fit by a sum of Lorentzians to determine the height, width, and position of each spectral feature. All transitions were adequately described by a single Lorentzian accept those observed in the NH_3 2^4 band. This system demonstrated a regular asymmetry that prevented a quantitative treatment of these transitions. The transition frequencies determined from the fits are given in tables I, II, III, and IV. As an example of the quality of the fits, in figure 6 are presented the calculated and observed transitions for the $J_K = 3_2$ rotational level in the NH_3 2^1 band. The observed widths are much larger than the laser bandwidth (0.4 cm^{-1}) or the Doppler width (0.1 cm^{-1}) and are therefore, a direct measure of the predissociation lifetime. These widths as they relate to the predissociation rates will be presented and discussed in the following paper [11].

The transition frequencies for the pure isotopomers, NH_3 and ND_3, were fit to a rigid symmetric top spectrum constraining the ground state constants to the literature values. In these fits, each observed transition frequency was weighted by the squared uncertainty from the lineshape fits. However, some of the lineshape fits yielded unreasonably small error estimates causing these transitions to be weighted too heavily. To correct this problem, a constant term that reflected systematic errors was added to the fit uncertainty for each transition frequency included. This constant was chosen to equate the χ^2 for the fit to the number of degrees of freedom. Fits were then redone with the new weights, and the process iterated until convergence. The rotational constants determined by this procedure are presented in table V and table VI along with previous determinations. Where a comparison can be made, our results agree favorably with other reports [4,5,17]. Additionally, two more points should be noted. First, we determine C better than the other rotational constants due to the predominance of high K levels in our data set. And second, the broad transition widths of the hydrogen containing isotopomers limited the accuracy of the experimental transition frequencies. Therefore, in these cases, distortion constants were not included in these fits.

One of the goals of the present work was the determination of the centrifugal distortion constants for the lowest two ND_3 vibronic bands. At first, a six parameter fit to determine the three distortion constants, D_{J^2}, D_{JK}, and D_{K^2}, was performed; results from these fits are given in column 1 of table VI. The parameters from the fits yielded unphysical values and were moderately correlated. Thus, utilizing relationships among the distortion constants for a planar symmetric top, a five parameter fit to τ_{xxxx} and τ_{zzzz} was also performed and results from these fits are reproduced in column 2 of table VI. A four parameter fit where τ_{zzzz} was constrained to zero was also performed for the 2^1 level as shown in column 3 of table VI. Results from these fits will be further elaborated in the discussion section.

The observed inertial defects for the NH_3 and ND_3 vibronic levels is given in table VII. These quantities were fit to $\Delta_{obs} = \Delta_o + \Delta_{\nu_2}(\nu_2 + 1/2)$ to determine the dependence on ν_2 excitation. The determined values for Δ_o and Δ_{ν_2} are also presented in table VII. These values were used in the fits of the mixed isotopomer data as discussed below.

The transition frequencies for the mixed isotopomers was fit to a rigid asymmetric top spectrum. Due to the limited number of observed transitions for these two species, all three rotational constants could not be determined independently. To improve these fits, we constrain the calculated inertial defect for the two mixed isotopomers to lie between

the values observed for the two pure isotopomers. As an example for the NH_2 2^1 level, we constrain the inertial defect to the following,

$$\Delta_{mixed} = \frac{2\Delta(NH_3, \nu_2 = 1) + \Delta(ND_3, \nu_2 = 1)}{3}. \quad (1)$$

B and C were independently varied while A was constrained to reproduce this calculated inertial defect. The determined values from these fits are presented in table V.

From the fit of the RFODR data on ND_3, we obtained preliminary rotational constants for the 2^1 band. Using these constants, including estimates for the J, K dependence of the width to be discussed in the following paper [11], the fluorescence excitation spectrum of the 2^1 band was simulated. This procedure allowed assignment of many of the strong features in the excitation spectrum, particularly the P branch. These assigned lines were used in the final refinement of the rotational constants of the 2^1 band. The simulation of the 2^1 band, using the final constants, is overlaid with the experimental spectrum in figure 5.

IV. DISCUSSION

In the previous $\tilde{A}$ state ammonia work, there have been substantial differences in the experimental [3,4] and theoretical [9,13] determinations of the $\tilde{A}$ state equilibrium bond length. The resolution of this controversy was one of the primary goals of the present work. Using the MODR technique, rotational constants were obtained for all the vibronic bands studied. Given the D_{3h} planar equilibrium structure of the $\tilde{A}$ state [3], there is only one structural parameter, the N–H equilibrium bond length, which in principle could be determined from the B or C rotational constants. The effective bond lengths derived through the B rotational constant data varied considerably, likely due to significant vibration - rotation interactions induced by b axis rotation. The effective bond lengths obtained from the C rotational constants showed less variation. Hence, we have estimated the equilibrium bond lengths by attempting to correct for the smaller vibration-rotation interactions in the observed C rotational constants.

For the two pure isotopomers, we used the fitted rotational constants in the ν_2=0 and ν_2=1 vibronic levels to calculate α_2^C. For NH_3, α_2^C was determined to be -0.07(5) cm^{-1} while for ND_3 it was -0.036(8) cm^{-1}. These values were used to correct for vibration-rotation effects caused by ν_2 excitation. After correction for this motion, an averaged bond length, r_o, was calculated for both species. For NH_3, r_o was determined to be 1.082(3) Å while for ND_3 it was 1.074(1) Å. For the remaining modes, $r_o - r_e$ should essentially scale as the inverse square root of the reduced mass [30]. For these two bands, the effects of the bend-stretch Fermi resonance (which is responsible for the rapid rise in the dissociation rate for levels with $\nu_2 > 1$) does not play a significant role. Thus, assuming the reduced mass of the remaining modes is dominated by H(D), we can extrapolate the above r_o values for NH_3 and ND_3 to yield a value for r_e of 1.055(8) Å. This result is in quantitative agreement with the *ab initio* value determined by Rosmus and co-workers [13], and confirms their suggestion that the apparent disagreement between theory and experiment was due to the neglect of vibration-rotation interactions in deducing the bond length from the accurately determined rotational constants of Douglas [4]. It is interesting to note that Douglas pointed out that

his estimated bond length had an unknown uncertainty, but this caveat was dropped in almost all subsequent references to this 'experimental' bond length.

Another goal of the present work was the experimental determination of the $\tilde{A}$ state harmonic force constants. There exist *ab initio* estimates of a few of these constants [13,31], but none have been experimentally determined. Due to the redundancy condition on the in-plane angles, the in-plane force field is described by only four constants, f_{rr}, $f_{rr'}$, $f_{\alpha\alpha} - f_{\alpha\alpha'}$, and $f_{\alpha r} - f_{\alpha r'}$. The out-of-plane force field is described by a single force constant, f_{hh}. To first order, two of these force constants, $f_{rr'}$ and $f_{\alpha r} - f_{\alpha r'}$, would only split the mode frequencies. Furthermore, assuming these constants to be reasonably close to the values of the electronic ground state [32], we anticipate these to be small and have little effect on the observed frequencies. In fact, comparison of the Q_1 and r(NH) *ab initio* potentials of McCarthy *et al.* [31] predict that $f_{rr'}$ is less than 0.1 aJ/Å^2. Initially, we take these force constants to be zero leaving only three force constants to be determined.

We had hoped that we could use the centrifugal distortion constants to help determine the harmonic force field. For both the ND_3 2^0 and 2^1 bands, we have accurately determined the rotational constants as well as the centrifugal distortion constants, D_J, D_{JK}, and D_K. Unfortunately, we were unable to use the same procedure to determine the centrifugal distortion constants for the 2^2 band due to the larger observed transition widths. We note that for a planar symmetric top, the centrifugal distortion constants are related by [33]

$$D_{JK} = -\frac{2}{3}(D_J + 2D_K). \tag{2}$$

The fits were constrained to obey this relationship. The centrifugal distortion constants are related to the force constants by [33]:

$$\tau_{xxxx} = -4D_J = -\frac{1}{2}(4\pi B)^4 \sum_{i,j} [J_{xx}^{(i)}]_e f_{ij}^{-1} [J_{xx}^{(j)}]_e \tag{3}$$

$$\tau_{zzzz} = \frac{4}{3}(D_K - D_J) = \frac{1}{2}(4\pi C)^4 (\frac{2}{3} m r^2)^2 f_{rr}^{-1} \tag{4}$$

where $[J_{xx}^{(i)}]_e = \delta I_{xx}/\delta Q_i$ at the equilibrium geometry. Our observed transition frequencies were then used to determine τ_{xxxx} and τ_{zzzz} for all three bands. These values are also included in table VI.

The τ_{xxxx} values listed in table VI for the 2^1 and 2^2 bands implies a negative value for $f_{\alpha\alpha} - f_{\alpha\alpha'}$. This result is clearly unphysical. In addition, f_{rr} from equation 2 for the 2^1 level, was calculated to be only 0.73 aJ/ Å^2. This value is in sharp disagreement with both the *ab initio* value and as discussed later, the value obtained by consideration of the observed zero point energies. We have clearly determined anomalous centrifugal distortion constants.

Anomalous centrifugal distortion constants often arise when a vibrational state is perturbed by a nearby level. In the present case, no such level appears available. For the 2^1 level, τ_{xxxx} appears to be poorly determined. However, in a fit without distortion constants, all the low J transitions have positive residuals while all the high J transitions have negative residuals. D_J must certainly be negative! Therefore, the centrifugal distortion constants obtained cannot be used to derive physically meaningful harmonic force constants.

The determination of the harmonic force field had to be obtained in a less direct manner. From the observed ν_2 vibrational progressions, we determine the out-of-plane bending force constant, f_{hh}. Since the higher members of the ν_2 progression are broad and erratically spaced [8], we use only the data from the 2^0, 2^1, and 2^2 band systems. From these levels for each of our isotopomers, ν_2 and X_{22} were determined. These values are presented in table VIII. Since the X_{22} values are small, the ν_2 frequencies are expected to scale as the inverse square of the reduced mass [30]. However, as the reduced mass is increased, the effective force constants systematically decrease; the force constant obtained from the ND_3 progression underestimates the NH_3 ν_2 fundamental frequency by approximately 40 cm^{-1}. We were able to still reasonably estimate f_{hh} at 1.06(4) aJ/ Å^2, nearly double the *ab initio* value of 0.66 aJ/ Å^2 [13].

Next, the in-plane force constant, $f_{\alpha\alpha} - f_{\alpha\alpha'}$, was determined. We can use the observed inertial defects to estimate this force constant. The inertial defect, $I_C - 2I_B$, is given for the 2^0, 2^1, and 2^2 vibronic levels for the two pure isotopomers in table VII. We assume that the centrifugal and electronic contributions to the inertial defect are small in comparison to the vibrational contribution and neglect their effect entirely. Therefore, the inertial defect was fit to [34]:

$$\Delta_{vib} = \sum_s \frac{h}{\pi^2 c}(\nu_s + \frac{1}{2}) \sum_{s'} \frac{\omega_{s'}^2}{\omega_s(\omega_s^2 - \omega_{s'}^2)}[(\zeta_{ss'}^{(x)})^2 + (\zeta_{ss'}^{(z)})^2 - (\zeta_{ss'}^{(y)})^2] + \sum_t \frac{h}{\pi^2 c}\frac{3}{2\omega_t}(\nu_t + \frac{1}{2}). \quad (5)$$

This inertial defect depends principally upon ν_2 and ν_4 and only very weakly on the other modes. Since ν_2 has already been accurately determined, analysis of the inertial defect should be a sensitive method to determine $f_{\alpha\alpha} - f_{\alpha\alpha'}$. Using the *ab initio* value for f_{rr} of 5.09 aJ/ Å^2 [13], and our calculated value for f_{hh}, we fit to the observed inertial defects and determine $f_{\alpha\alpha} - f_{\alpha\alpha'}$ to be 0.25(2) aJ. The calculated inertial defects are also included in table VII for comparison. It should be mentioned that this value for $f_{\alpha\alpha} - f_{\alpha\alpha'}$ is significantly lower than the ground state value of 0.68 aJ/ Å^2 [32]. Changing the assumed value of f_{rr} by 20% changes the calculated inertial defect by <0.5%.

The calculated inertial defects demonstrated systematic errors from the observed ND_3 values. Even changing the f_{hh} force constant considerably while varying $f_{\alpha\alpha} - f_{\alpha\alpha'}$ could not reproduce the large positive inertial defect we observed for the ND_3 2^0 level. In our approach, we have neglected centrifugal contributions to the inertial defect. This contribution is given by [34]

$$\Delta_{cent} = -\hbar^4 \tau_{zxzx}(\frac{3}{4}\frac{I_{yy}}{C} + \frac{I_{xx}}{2B} + \frac{I_{zz}}{2A}).$$

This contribution is predicted to be on the order of 10^{-3} and far too small to explain our large deviation from the observed values. We suggest that perturbations in this level are causing τ_{zxzx} to be anomalously large such that the centrifugal contributions to the inertial defect are much larger than predicted. However, since the observed inertial defects for NH_3 are well reporduced as well as the relative spacings for the ND_3 levels, we feel that our determined value for $f_{\alpha\alpha} - f_{\alpha\alpha'}$ is reasonably close to the true value.

Now we turn attention to the perturbation observed in the NH_3 2^4 band. It had been suggested that this asymmetry reflected a partially resolved structure built off one quantum in the ν_1 mode [8]; thus, the 2^4 band system would be overlapped by the $1^1 2^1$ band system. The 2^4 and $1^1 2^1$ vibronic levels have opposite symmetry with respect to reflection in the

plane, and thus can not interact through anharmonic interactions. Furthermore, the $1^1 2^1$ assignment can be ruled out by the phase of the observed MODR signals. Transitions to the 2^4 level originate from symmetric levels in the ground electronic state (leading to an initial emission of the microwave radiation) while transitions to the $1^1 2^1$ level arise from asymmetric levels (leading to absorption). Thus, the phase of the MODR signal from these two transitions would have opposite signs. Since the observed asymmetry in the 2^4 MODR spectrum was the same as in absorption, this asymmetry is not the result of the $1^1 2^1$ band.

The observation of this asymmetry implies a coupling of the ν_2 mode that is greater than its coupling with the dissociative continuum. If the mode attributable to this perturbation were either of the stretching modes, the dissociation rate from the quasibound state would have been enhanced greatly; hence, broader lines would have been expected than what we observed. The only other mode that could be responsible for the observed perturbation is due to ν_4, the degenerate in-plane bending mode. Using the above value for $f_{\alpha\alpha} - f_{\alpha\alpha'}$ we predict that the harmonic frequency for ν_4 is 1114 cm^{-1}. We assign the observed perturbation of the 2^4 level to an anharmonic mixing with the A_1 component of the 4^3 levelnad thus, the two levels are brought into resonance assuming ν_4 = 1114 cm^{-1} and X_{44} = 25 cm^{-1}. We have neglected the contribution of g_{44} for lack of data. The 4^3 level has a harmonic amplitude of $\pm$ 43 degrees so we would expect a substantial positive anharmonic correction due to the steric repulsion of the hydrogen atoms.

We are then left with only one force constant, f_{rr}, to determine. To estimate this force constant, we use our observed isotopic shifts in band origins. This shift results from changes in vibrational zero point energy due to isotopic substitution. We assume the harmonic approximation and use,

$$T_o = T_e + E_o^{upper} + E_o^{lower} \tag{6}$$

where T_o is the observed 0-0 band origin for a given isotopomer, T_e is the energy difference between the two potential surface minima, and E_o^{upper} and E_o^{lower} are the zero point energies for the $\tilde{A}$ and $\tilde{X}$ states respectively. E_o^{lower} is taken from the *ab initio* work of Hargiss and Ermler [32] while T_o was known for each of our isotopomers. Constraining T_e to be constant and utilizing our determined values for the other $\tilde{A}$ state force constants, f_{rr} was varied to reproduce the observed band origins for the two pure isotopomers. We then used the T_o values for the mixed isotopomers as a consistency check. Using this procedure, f_{rr} was determined to be 4.2 aJ/ Å^2 while T_e was found at 48070 cm^{-1}.

The determined value for f_{rr} is approximately 80% of the value determined by Rosmus and coworkers [13]. We attribute this discrepancy to a neglect of anharmonicity in the excited state potential. In order to estimate these effects, we use the *ab initio* values for X_{NH} = -236 cm^{-1} and X_{ND} = -118 cm^{-1} and correct for the anharmonicity of the excited state. After this correction, f_{rr} was readjusted to 4.9 aJ/ Å^2 in better agreement with the it ab initio results [13]. Our estimated values of the force constants, T_e, and the vibrational frequencies for all four isotopomers are presented in table IX.

To estimate any effect due to the neglect of $f_{\alpha r} - f_{\alpha r'}$ and $f_{rr'}$ on the observed zero point energies, we insert these into the above calculations and redetermine our T_e and f_{rr} values. Inclusion of $f_{rr'}$ at its ground state value of 0.31 aJ/ Å^2 changes the calculated T_e values by a uniform 14 cm^{-1}. Likewise, addition of $f_{\alpha r} - f_{\alpha r'}$ at its ground state value of -0.176 aJ increases T_e by a uniform 20 cm^{-1}. Therefore, the neglect of these two force constants

has little effect on our calculated values for f_{rr} and T_e. In addition, increasing f_{rr} by 0.1 aJ/ Å^2 changes $T_e(NH_3)$ - $T_e(ND_3)$ by 14 cm^{-1}. Hence, this method is a sensitive measure of the f_{rr} force constant. Given the above sensitivities to unknown potential parameters, we suggest that $T_e = 48070 \pm 200$ cm^{-1}. The *ab initio* predictions for T_e were 44260 cm^{-1} (CASSCF) and 45380 cm^{-1} (CEPA) respectively.

The NH_3 and ND_3 ν_1 frequencies calculated from the derived harmonic force field agrees very well with the *ab initio* determined values [13,31]. These values are about 500 cm^{-1} higher than the values assigned to the fundamentals through dispersed fluorescence from the $\tilde{C}'$ state [10]. While the anharmonic corrections to the fundamental frequency are quite large, the ν_1 fundamental is above the barrier to dissociation along one N–H bond, and as discussed in the following paper, we believe it should be extremely diffuse. We propose to reassign the broad features observed by Ashfold *et al.* [10] to the 4^2 band. On the basis of our above values for ω_4 and X_{44}, we predict the 4^2 band should lie near 2425 cm^{-1} compared to 2350 cm^{-1} for the center of the feature previously assigned as 1^1. The width, and perhaps a downward shift of the 4^2 band, we believe to arise from an anharmonic mixing of this level with the continuum created by the N–H bond dissociation. From our harmonic force field, we predict that the ND_3 4^2 band should lie at 1730 cm^{-1}. In the ND_3 dispersed fluorescence spectrum [10], a broad but highly asymmetric feature was observed at 1790 ± 50 cm^{-1} and assigned to the 1^1 band very near to our predicted value for the 4^2 band.

With this newly determined value for ω_4, we had hoped that a progression built from this mode could be directly observed in the fluorescence excitation spectrum of ND_3. While this level is not Franck-Condon active, the large Coriolis interaction between modes ν_2 and ν_4 predicted by the above force field will give intensity to the upper J levels of the 4^1 band. However, in the expected region, an overlapping ν_2 hot band transition made direct observation of this mode difficult. Still an extremely weak and broad transition lying approximately 815 cm^{-1} above the band origin was observed in the wings of the hot band transition that we have assigned to the ν_4 mode. It should be noted that the signal to noise ratio was low and thus the assignment is tentative.

V. CONCLUSION

We have demonstrated the MODR technique used previously to investigate the vibrational overtones of ammonia can also be effectively used to investigate the predissociative $\tilde{A}$ state electronic spectrum. Using this method, we have recorded the electronic spectrum of NH_3, NH_2D, and NHD_2 with rotational resolution. Our results for NH_3 represent a significant improvement upon previous experimental results [4,10,17] while the results for the mixed isotopomers represent the first high resolution studies of these species. To investigate ND_3 with the same resolution as the hydrogen containing species, a strip-line cell was constructed that allowed the simultaneous passage of radio-frequency and ultraviolet radiation. We have used this cell to record the electronic spectrum of ND_3 with improved rotational resolution. Thus far, these results represent the most thorough spectroscopic investigation of the $\tilde{A}$ state electronic spectrum.

We have used the rotational constants derived from individual rovibrational transitions to determine the ammonia $\tilde{A}$ state equilibrium bond length. We estimate this bond length to be 1.055(8) Å. This value is significantly different from the previous experimentally determined

values [3,4] but is quite close to the *ab initio* value of Rosmus and coworkers [13]. In addition, for the first time, the $\tilde{A}$ state harmonic force field has been experimentally estimated. Where applicable, these estimates were compared to the *ab initio* determined values [13,31]. From the calculated vibrational term values, we predict f_{hh} is 1.06(4) aJ/ Å^2, nearly double the value determined by Rosmus *et al.* [13]. Using the observed inertial defects, we predict $f_{\alpha\alpha} - f_{\alpha\alpha'}$ to be 0.25(2) aJ and f_{rr} was found to be 4.9 aJ/ Å^2 through consideration of the shifts in band origin upon isotopic substitution. f_{rr} agrees well with the value determined through the *ab initio* work while $f_{\alpha\alpha} - f_{\alpha\alpha'}$ is approximately 40% of the ground state value [32].

Strong asymmetry was observed in rovibronic transitions to the $\tilde{A}$ state 2^4 level. This asymmetry has been attributed to a strong anharmonic resonance with the 4^3 level. Attempts to estimate the force constants more directly by analysis of the centrifugal distortion constants failed. Anomalous centrifugal distortion constants were obtained for both the ND_3 2^0 and 2^1 levels indicating significant interaction with a nearby level.

REFERENCES

[1] S. A. Henck, *The $\tilde{A}$ state of Ammonia and Coherence Transfer between Rotation-Inversion Transitions in Ammonia*, PhD thesis, Princeton University, 1990.

[2] S. W. Leifson, *Astrophysics Journal* **63**, 73 (1933).

[3] A. D. Walsh and P. A. Warshop, *Trans. Faraday Soc.* **57**, 345 (1961).

[4] A. E. Douglas, *Dis. Faraday Soc.* **35**, 158 (1963).

[5] L. D. Ziegler and B. Hudson, *J. Phys. Chem.* **88**, 1110 (1984).

[6] T. A. Gregory and S. Lipsky, *J. Chem. Phys.* **65**, 5469 (1976).

[7] W. R. Harshbarger, *J. Chem. Phys.* **53**, 903 (1970).

[8] V. Vaida, M. I. McCarthy, P. C. Engelking, P. Rosmus, H. J. Werner, and P. Botschwina, *J. Chem. Phys.* **86**, 6669 (1987).

[9] S. L. Tang and D. G. Imre, *Chem. Phys. Let.* **144**, 6 (1988).

[10] M. N. R. Ashfold, C. L. Bennett, and R. N. Dixon, *Faraday Discuss. Chem. Soc.* **82**, 163 (1986).

[11] S. A. Henck, M. A. Mason, W.-B. Yan, and K. K. Lehmann, Microwave detected, microwave-optical double resonance of NH_3, NH_2D, NHD_2, and ND_3: II. Predissociation dynamics of the $\tilde{A}$ State., Accepted in J. Chem. Phys.

[12] S. L. Tang, D. G. Imre, and D. Tannor, *J. Chem. Phys.* **92**, 5919 (1990).

[13] P. Rosmus, P. Botschwina, H. J. Werner, V. Vaida, P. C. Engelking, and M. I. McCarthy, *J. Chem. Phys.* **86**, 6677 (1987).

[14] S. L. Tang, E. V. Abramson, and D. G. Imre, *J. Phys. Chem.* **95**, 4969 (1991).

[15] M. N. R. Ashfold, C. L. Bennett, R. N. Dixon, P. Fielden, H. Rieley, and R. J. Stickland, *J. Mol. Spec.* **117**, 216 (1986).

[16] R. N. Dixon, *Chem. Phys. Let.* **147**, 377 (1988).

[17] J. Xie, G. Sh, X. Zhang, and C. Zhang, *Chem. Phys. Let.* **124**, 99 (1986).

[18] L. D. Ziegler, *J. Chem. Phys.* **82**, 664 (1985).

[19] S. L. Coy and K. K. Lehmann, *J. Chem. Phys.* **84**, 5239 (1986).

[20] A. H. Sharbaugh, T. C. Madison, and J. K. Bragg, *Physical Review* **76**, 1529 (1949).

[21] W. E. Good and K. K. Coles, *Phys. Rev.* **71**, 383 (1947).

[22] C. Townes and A. H. Schawlow, *Microwave Spectroscopy*, Dover Publications, New York, 1955.

[23] G. Hermann, *J. Chem. Phys.* **29**, 875 (1958).

[24] F. C. Delucia and P. Helminger, *J. Mol. Spec.* **54**, 200 (1975).

[25] L. Fusina, G. di Lonardo, and J. W. C. Johns, *J. Mol. Spec.* **112**, 211 (1985).

[26] Y. Endo, M. Iida, and Y. Ohshima, *Chem. Phys. Let.* **174**, 401 (1990).

[27] M. A. Mason and K. K. Lehmann, *J. Chem. Phys.* **98**, 5184 (1993).

[28] F. M. Phelps, editor, *M. I. T. Wavelength Tables*, M. I. T. Press, Cambrige, MA, 1982.

[29] J. C. Cariou and P. Luc, *Atlas du Spectre D'Absorption De La Molecule De Tellure*, Laboratoire Aime-Cotton CNRS II, Orsay, France, 1980.

[30] V. W. Laurie, *J. Chem. Phys.* **28**, 704 (1958).

[31] M. I. McCarthy, P. Rosmus, H. J. Werner, P. Botschwina, and V. Vaida, *J. Chem. Phys.* **86**, 6693 (1987).

[32] L. O. Hargiss and W. C. Ermler, *J. Phys. Chem.* **92**, 300 (1988).

[33] W. Gordy and R. L. Cook, *Microwave Molecular Spectra*, John Wiley and Sons, New York, 1984.
[34] T. Oka and Y. Morino, *J. Mol. Spec.* **6**, 472 (1961).

TABLES

TABLE I. Frequencies of the NH_3 $\tilde{A} \leftarrow \tilde{X}$ state transitions observed by MODR.

2^0 band.

Transition	ν_o **(cm^{-1})**	**1σ**
$Q_2(2)$	46144.370	0.037
$R_2(2)$	46201.910	0.115
$Q_3(3)$	46137.020	0.028
$R_3(3)$	46214.420	0.127
$Q_4(4)$	46127.340	0.065
$R_4(4)$	46225.220	0.456
$Q_4(5)$	46125.220	0.147
$R_4(5)$	46238.290	1.782
$Q_5(5)$	46114.120	0.052
$R_5(5)$	46228.680	0.495
$Q_6(6)$	46098.280	0.049
$R_6(6)$	46230.880	0.797
$P_6(7)$	45958.160	0.842
$Q_6(7)$	46095.960	0.078
$R_6(7)$	46251.720	0.590
$Q_7(7)$	46079.610	0.076
$R_7(7)$	46234.240	0.545
$Q_8(8)$	46058.270	0.060
$R_8(8)$	46233.910	1.113
$Q_9(9)$	46034.510	0.224

2^1 band.

Transition	ν_o **(cm^{-1})**	**1σ**
$Q_1(1)$	47039.410	0.044
$R_1(1)$	47075.670	0.093
$P_2(3)$	46975.220	0.095
$Q_2(3)$	47029.730	0.029
$R_2(3)$	47101.370	0.046
$Q_3(3)$	47028.240	0.012
$R_3(3)$	47099.560	0.057
$P_2(5)$	46921.520	0.193
$Q_2(5)$	47010.530	0.274
$R_2(5)$	47121.470	0.158
$P_4(5)$	46918.020	0.091
$Q_4(5)$	47008.240	0.199
$R_4(5)$	47116.600	0.102
$Q_4(5)$	47007.310	0.037
$R_4(5)$	47113.960	0.370
$P_3(6)$	46890.820	0.254
$Q_3(6)$	46999.900	0.189
$R_3(6)$	47127.040	0.206

$P_5(6)$	46885.750	0.483
$Q_5(6)$	46991.660	0.049
$R_5(6)$	47118.030	0.306
$R_6(7)$	47119.680	0.277
$Q_7(8)$	46954.520	0.076
$Q_8(8)$	46949.130	0.018
$R_8(8)$	47111.080	0.409
$P_8(9)$	46763.110	2.098
$R_8(9)$	47113.430	1.158
$Q_9(9)$	46926.020	0.057
$R_9(9)$	47108.440	2.188

2^2 band.

Transition	ν_o **(cm^{-1})**	**1σ**
$Q_3(3)$	47926.520	0.140
$R_3(3)$	47991.890	0.590
$Q_6(6)$	47887.380	0.080
$R_6(6)$	48006.360	1.580

2^3 band.

Transition	ν_o **(cm^{-1})**	**1σ**
$Q_1(1)$	48857.500	0.260
$R_1(1)$	48890.700	0.520
$Q_2(2)$	48848.200	0.520
$R_2(2)$	48898.000	1.000
$Q_3(3)$	48836.600	0.180
$R_3(3)$	48903.000	0.360
$Q_3(4)$	48828.500	0.680
$R_3(4)$	48911.500	1.400
$P_3(4)$	48762.100	1.400
$Q_4(4)$	48826.300	0.190
$R_4(4)$	48907.600	0.380
$P_3(5)$	48721.300	0.470
$Q_3(5)$	48805.800	0.230
$R_3(5)$	48907.300	0.280
$Q_5(5)$	48815.200	0.280
$R_3(5)$	48912.800	0.560
$P_3(6)$	48689.900	1.100
$Q_3(6)$	48788.000	0.820
$R_3(6)$	48903.400	0.790
$Q_6(6)$	48800.200	0.190
$R_6(6)$	48916.400	0.380
$P_6(7)$	48671.300	0.730
$Q_6(7)$	48775.800	0.130
$R_6(7)$	48912.700	0.600
$Q_7(7)$	48788.000	0.140

$R_7(7)$	48930.200	2.400
$P_6(8)$	48616.100	0.760
$Q_6(8)$	48748.900	0.380
$R_6(8)$	48898.300	0.760

TABLE II. Frequencies of the NH_2D $\tilde{A} \leftarrow \tilde{X}$ state transitions observed by MODR.

2^0 band.

Transition	ν_o **(cm^{-1})**	**1σ**
$3_{03} \leftarrow 3_{13}$	46318.81	0.06
$4_{23} \leftarrow 3_{13}$	46377.17	0.27
$4_{14} \leftarrow 4_{04}$	46312.12	0.05
$5_{14} \leftarrow 4_{04}$	46382.77	0.37
$5_{15} \leftarrow 5_{05}$	46302.82	0.10
$6_{15} \leftarrow 5_{05}$	46386.90	0.76
$6_{06} \leftarrow 7_{16}$	46184.25	2.52
$7_{26} \leftarrow 7_{16}$	46292.49	0.31
$7_{07} \leftarrow 8_{17}$	46162.34	1.42
$8_{27} \leftarrow 8_{17}$	46277.10	0.10
$9_{27} \leftarrow 8_{17}$	46407.45	0.60

2^1 band.

Transition	ν_o **(cm^{-1})**	**1σ**
$3_{13} \leftarrow 3_{03}$	47131.70	0.02
$4_{13} \leftarrow 3_{03}$	47183.77	0.13
$4_{04} \leftarrow 4_{14}$	47123.14	0.10
$5_{24} \leftarrow 4_{14}$	47191.81	0.97
$5_{05} \leftarrow 5_{15}$	47114.68	0.06
$6_{25} \leftarrow 5_{15}$	47196.05	0.97
$6_{16} \leftarrow 7_{26}$	46999.00	0.60
$7_{16} \leftarrow 7_{26}$	47095.97	0.08
$8_{36} \leftarrow 7_{26}$	47207.14	0.38
$7_{17} \leftarrow 8_{27}$	46969.76	0.44
$8_{17} \leftarrow 8_{27}$	47081.86	0.05

2^2 band.

Transition	ν_o **(cm^{-1})**	**1σ**
$3_{03} \leftarrow 3_{13}$	47958.77	0.08
$4_{23} \leftarrow 3_{13}$	48016.74	0.45
$4_{14} \leftarrow 4_{04}$	47952.47	0.19
$5_{15} \leftarrow 5_{05}$	47942.78	0.08
$6_{15} \leftarrow 5_{05}$	48025.22	1.02
$7_{26} \leftarrow 7_{16}$	47918.55	0.34
$7_{07} \leftarrow 8_{17}$	47806.90	1.58
$8_{27} \leftarrow 8_{17}$	47904.42	0.15
$9_{27} \leftarrow 8_{17}$	48033.32	1.70

TABLE III. Frequencies of the NHD_2 $\tilde{A} \leftarrow \tilde{X}$ state transitions observed by MODR.

2^0 band.

Transition	ν_o **(cm^{-1})**	**1σ**
$2_{02} \leftarrow 2_{12}$	46508.41	0.07
$3_{22} \leftarrow 2_{12}$	46546.54	0.21
$3_{13} \leftarrow 3_{03}$	46505.93	0.10
$4_{13} \leftarrow 3_{03}$	46550.36	0.50
$4_{14} \leftarrow 5_{24}$	46438.30	0.48
$5_{14} \leftarrow 5_{24}$	46496.92	0.07
$6_{34} \leftarrow 5_{24}$	46569.67	0.23

2^1 band.

Transition	ν_o **(cm^{-1})**	**1σ**
$2_{12} \leftarrow 2_{02}$	47248.53	0.02
$3_{12} \leftarrow 2_{02}$	47279.38	0.07
$3_{03} \leftarrow 3_{13}$	47242.99	0.04
$4_{23} \leftarrow 3_{13}$	47288.89	0.19
$4_{04} \leftarrow 5_{14}$	47176.79	0.11
$5_{24} \leftarrow 5_{14}$	47233.86	0.02
$6_{24} \leftarrow 5_{14}$	47297.90	0.05

2^2 band.

Transition	ν_o **(cm^{-1})**	**1σ**
$2_{02} \leftarrow 2_{12}$	47994.52	0.13
$3_{22} \leftarrow 2_{12}$	48028.42	0.40
$3_{13} \leftarrow 3_{03}$	47991.77	0.19
$4_{13} \leftarrow 3_{03}$	48035.52	0.92
$4_{14} \leftarrow 5_{24}$	47923.51	0.45
$5_{14} \leftarrow 5_{24}$	47977.84	0.06
$6_{34} \leftarrow 5_{24}$	48042.56	0.20

TABLE IV. Frequencies of the ND_3 $\tilde{A} \leftarrow \tilde{X}$ state transitions observed by MODR.

2^0 band.

Transition	ν_o **(cm^{-1})**	**1σ**
$Q_3(3)$	46706.933	0.0442
$Q_4(4)$	46702.008	0.0430
$Q_3(5)$	46703.979	0.0558
$Q_5(5)$	46695.713	0.0190
$Q_6(6)$	46687.893	0.0229
$Q_6(7)$	46685.503	0.0444
$Q_7(7)$	46679.039	0.0172
$Q_6(8)$	46682.565	0.0248
$Q_7(8)$	46675.908	0.0236
$Q_8(8)$	46668.619	0.0117
$Q_6(9)$	46675.608	0.1147
$Q_9(9)$	46656.743	0.0312
$Q_9(10)$	46653.319	0.0293

2^1 band.

Transition	ν_o **(cm^{-1})**	**1σ**
$Q_1(1)$	47366.436	0.0204
$Q_2(2)$	47364.104	0.0267
$Q_3(3)$	47360.481	0.0095
$R_3(3)$	47360.481	0.0135
$Q_3(4)$	47357.568	0.0142
$Q_4(4)$	47355.529	0.0042
$R_4(4)$	47403.190	0.0319
$Q_3(5)$	47353.913	0.0264
$Q_5(5)$	47349.359	0.0164
$Q_3(6)$	47349.620	0.0253
$Q_5(6)$	47344.960	0.0165
$Q_6(6)$	47341.996	0.0086
$Q_6(7)$	47336.624	0.0091
$Q_7(7)$	47332.976	0.0066
$Q_6(8)$	47331.091	0.0103
$Q_7(8)$	47327.133	0.0256
$Q_8(8)$	47322.896	0.0057
$Q_3(9)$	47333.513	0.0657
$Q_6(9)$	47324.945	0.0468
$Q_9(9)$	47311.590	0.0155
$Q_9(10)$	47304.254	0.0129
$Q_9(11)$	47295.952	0.0235
$Q_{10}(11)$	47290.568	0.0273
$Q_{11}(12)$	47275.774	0.0225
$Q_{12}(14)$	47249.702	0.0382

2^2 band.

Transition	ν_o **(cm^{-1})**	**1σ**
$Q_3(3)$	48024.337	0.0528
$Q_3(4)$	48019.452	0.1298
$Q_4(4)$	48019.761	0.0940
$Q_3(5)$	48014.317	0.1770
$Q_5(5)$	48013.202	0.0768
$Q_6(6)$	48005.929	0.0704
$Q_6(7)$	47997.295	0.2152
$Q_7(8)$	47988.188	0.1127
$Q_9(9)$	47975.291	0.2514

TABLE V. Constants derived from rotational band fits of the $\tilde{A} \leftarrow \tilde{X}$ transitions in NH_3, NH_2D, and NHD_2.

	ν_2	ν_o**(cm^{-1})**	**A(cm^{-1})**	**B(cm^{-1})**	**C(cm^{-1})**
For NH_3.	0	46150(1)		9.71(6)	4.80(2)
				9.72[†]	4.79[†]
				9.6[‡]	4.8[‡]
	1	47042.2(8)		9.01(3)	4.87(2)
				9.05[†]	4.85[†]
				9.05[‡]	5.2[‡]
	2	47942(3)		8.4(3)	5.0(1)
				8.66[†]	4.87[†]
				8.5[‡]	5.4[‡]
	3	48856(2)		8.21(8)	4.98(8)
				8.4[b]	5.8[†]
	4	49978(5)			
For NH_2D.	0	46328.9(3)	8.9	6.37(30)	3.649(9)
	1	47141.38(13)	9.1	5.78(6)	3.737(5)
	2	47970.4(5)	7.8	5.9(6)	3.782(20)
For NHD_2.	0	46513.14(14)	7.3	5.06(4)	2.936(5)
	1	47251.58(9)	7.0	4.809(13)	2.987(3)
	2	47999.80(20)	6.2	4.88(10)	3.028(8)

[†]Reference [17]
[‡]Reference [18]

TABLE VI. Constants derived from rotational band fits of the ND_3 $\tilde{A} \leftarrow \tilde{X}$ transitions.

	Constant	**Fit I**	**Fit II**	**Fit III**
2^0 band.	ν_o	46713.6(2)	46713.3(1)	
	B	5.02(2)	5.04(1)	
	C	2.431(9)	2.438(2)	
	D_J **(x 10^4)**	26.(3)		
	D_{JK} **(x 10^4)**	-57.(5)		
	D_K **(x 10^4)**	30.(3)		
	τ_{xxxx} **(x 10^4)**		-109.(10)	
	τ_{zzzz} **(x 10^4)**		0^a	
	σ_{err}	0.18	0.17	
2^1 band.	ν_o	47367.51(5)	47357.50(5)	47367.60(9)
	B	4.772(4)	4.768(4)	4.785(8)
	C	2.4745(19)	2.4779(17)	2.465(1)
	D_J **(x 10^4)**	-2.0(7)		
	D_{JK} **(x 10^4)**	7.0(15)		
	D_K **(x 10^4)**	-4.9(9)		
	τ_{xxxx} **(x 10^4)**		8.0(29)	-12.(5)
	τ_{zzzz} **(x 10^4)**		-2.09(24)	$0.^a$
	σ_{err}	0.1	0.12	0.21
2^2 band.	ν_o	48031.9(2)	48032.2(4)	
	B	4.57(2)	4.40(8)	
	C	2.489(6)	2.52(2)	
	D_J **(x 10^4)**	$0.^a$		
	D_{JK} **(x 10^4)**	$0.^a$		
	D_K **(x 10^4)**	$0.^a$		
	τ_{xxxx} **(x 10^4)**		295.(120)	
	τ_{zzzz} **(x 10^4)**		-10.(7)	
	σ_{err}	0.33	0.23	

Numbers in parentheses are $\pm 1\sigma$.
All values given are in wavenumbers.
[a]Constrained value.
σ_{err} represents the systematic error. It is added in quadrature to the statistical error of each fitted line to make χ^2 for the fit equal to the number of degrees of freedom.

TABLE VII. Observed and calculated inertial defects for the two 'pure' isotopomers, NH_3 and ND_3. Numbers in parantheses are $\pm 2\sigma$.

For ND_3.	**Observed (amu-Å^2)**	**Calculated (amu-Å^2)**
2^0 band	+0.218(25)	+0.083
2^1 band	-0.264(9)	-0.326
2^2 band	-0.61(3)	-0.736

$$\Delta_{obs} = 0.39(3) - 0.42(2)(\nu_2 + \tfrac{1}{2})$$

For NH_3.	**Observed (amu-Å^2)**	**Calculated (amu-Å^2)**
2^0 band	+0.04(2)	+0.064
2^1 band	-0.28(2)	-0.232
2^2 band	-0.6(2)	-0.511

$$\Delta_{obs} = 0.19(3) - 0.30(3)(\nu_2 + \tfrac{1}{2})$$

TABLE VIII. Out-of-plane vibrational frequencies and anharmonic constants.

	Transition	$\nu_2(\mathrm{cm}^{-1})$	$2\chi_{22}(\mathrm{cm}^{-1})$
For NH_3.			
	$2^1 \leftarrow 2^0$	892	
	$2^2 \leftarrow 2^1$	900	8
	$2^3 \leftarrow 2^2$	914	14
	$2^4 \leftarrow 2^3$	942	28
For NH_2D.			
	$2^1 \leftarrow 2^0$	812.9	
	$2^2 \leftarrow 2^1$	830.1	17.2
	$2^3 \leftarrow 2^2$	855	24.9
For NHD_2.			
	$2^1 \leftarrow 2^0$	738.3	
	$2^2 \leftarrow 2^1$	748.4	10.1
	$2^3 \leftarrow 2^2$	763.5	15.1
For ND_3.			
	$2^1 \leftarrow 2^0$		
	$2^1 \leftarrow 2^0$		10.5

TABLE IX. Calculated $\tilde{A}$ state normal mode frequencies derived from the experimentally determined force field. All values are given in cm^{-1}. Values given in parentheses are worst case estimates.

Mode	**NH_3**	**NH_2D**	**NHD_2**	**ND_3**
ν_1	2870.(30)	2930.(30)	2980.(30)	2030.(20)
ν_2	892.(4)	813.(50)	738.(20)	653.(10)
ν_3	3020(30)	3020.(30)	2094.(21)	2244.(23)
		2165.(25)	2245.(24)	
ν_4	1110.(50)	1110.(50)	1020.(50)	820.(40)
		930.(40)	820.(40)	
		Zero Point Energy		
	5840.(200)	5340.(180)	4830.(180)	4310.(170)
		T_e		
	48071.30	48070.63	48064.96	48070.53

FIGURES

FIG. 1. Schematic diagram of the microwave detected, microwave- optical double resonance spectrometer.

FIG. 2. Microwave absorption observed from the NH_2D $3_{13}, 0 \leftarrow 3_{03}, 1$ inversion level following pumping of the lower level by a resonant ultraviolet pulse.

FIG. 3. Observed MODR signal to the 2^3 and 2^4 levels in the NH_3 $\tilde{A}$ state with the microwave frequency locked on the ground state 6_6 inversion doublet. The parallel polarization of the two fields and Honl-London factors permit observation of only the Q branches.

FIG. 4. Cross section of the RFODR cell. The strip-line is held at a fixed distance from the ground plane by specially machined KEL-F blocks. The laser is passed between the strip-line and the ground plane.

FIG. 5. Calculated and observed fluorescence excitation spectrum of the ND_3 2^1 band.

FIG. 6. The observed and calculated transitions for the $J_K = 3_2$ rotational level in the NH_3 2^1 band.

Figure 3

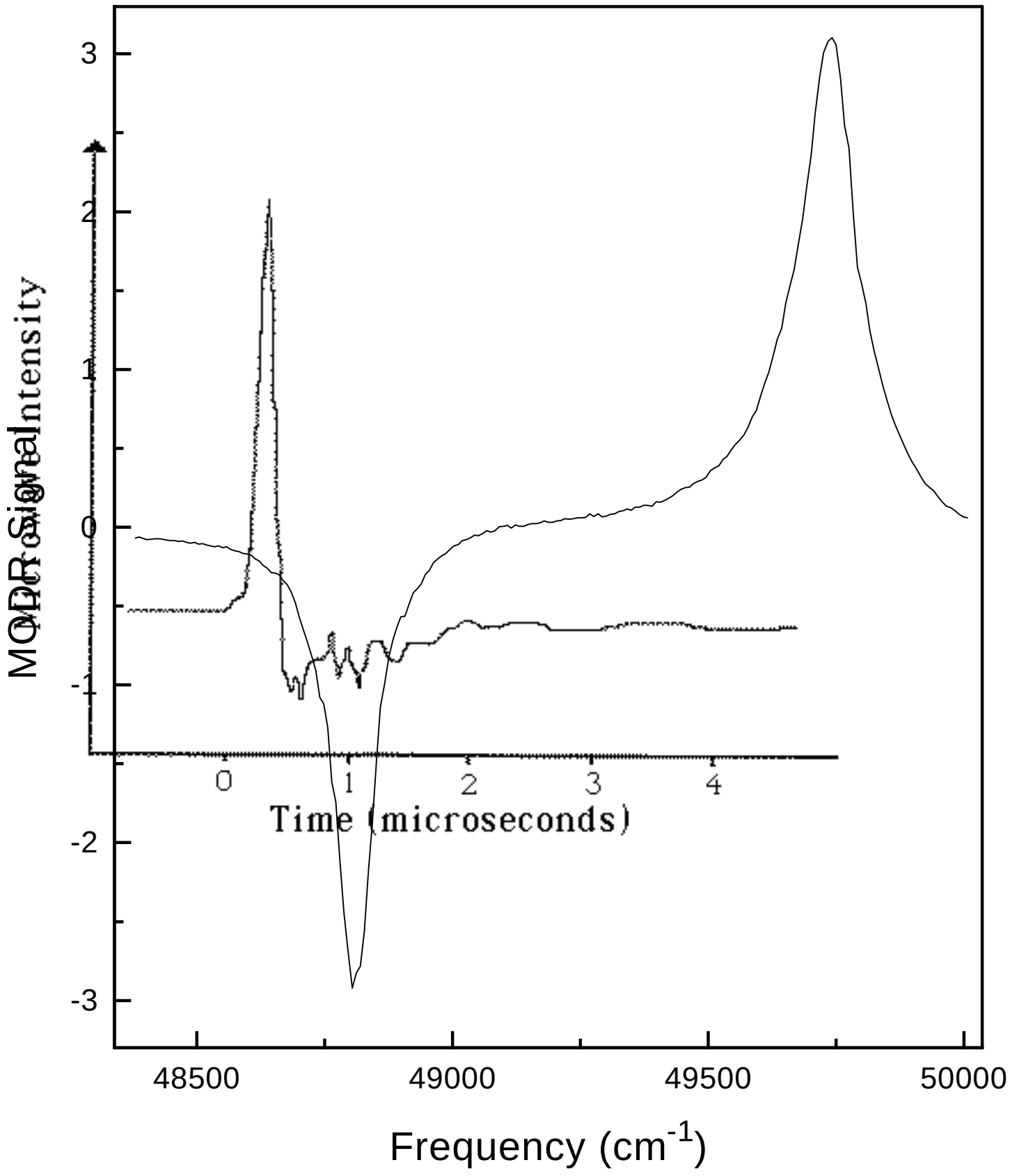
MODR Signal Intensity
3
2
1
0
-1
-2
-3
0
1
2
3
4
Time (microseconds)
48500
49000
49500
50000
Frequency (cm-1)

Figure 5

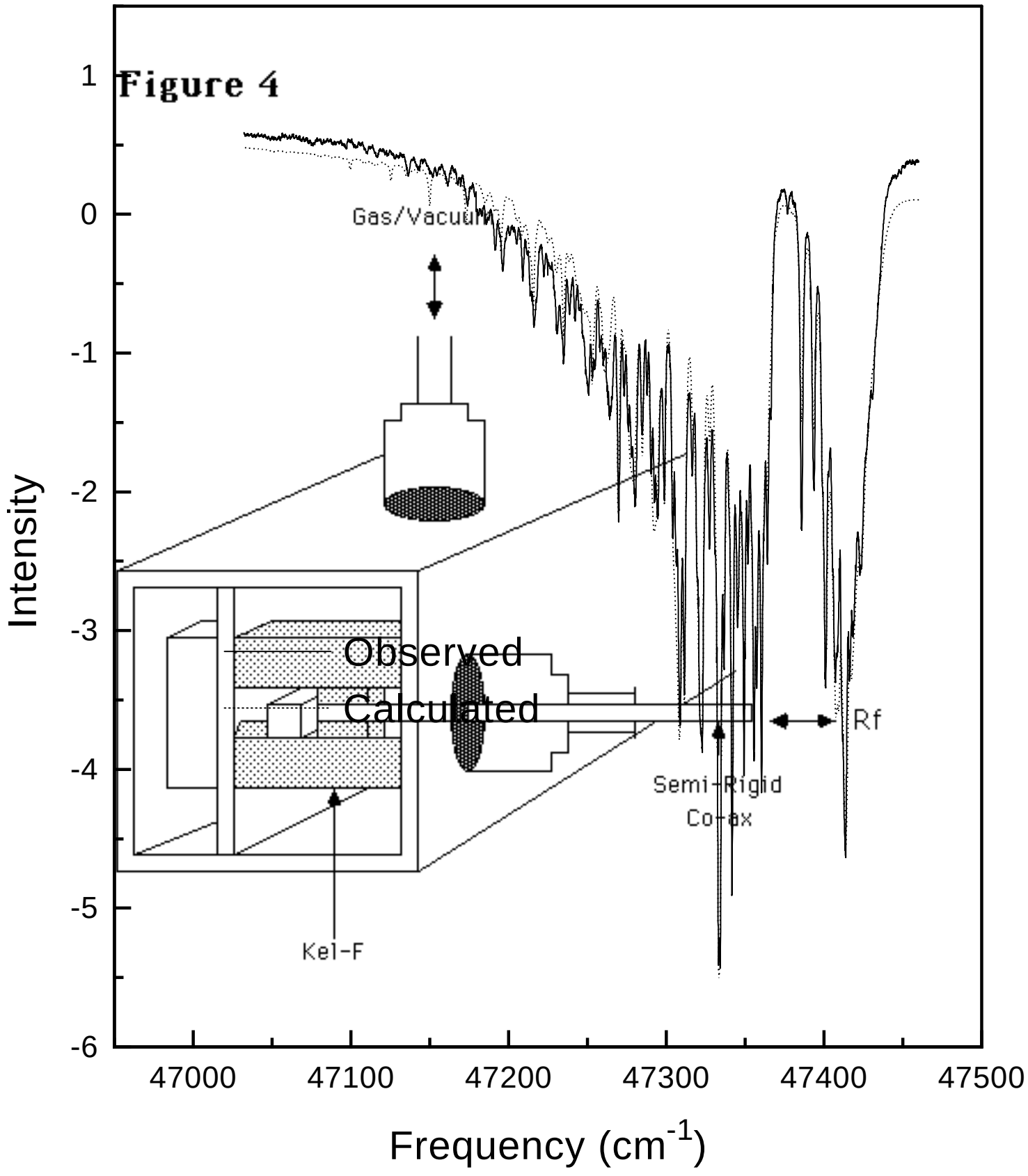
Figure 4
Gas/Vacuum
Observed
Calculated
Rf
Semi-Rigid
Co-ax
Kel-F
Intensity
Frequency (cm-1)
1
0
-1
-2
-3
-4
-5
-6
47000
47100
47200
47300
47400
47500

Figure 6

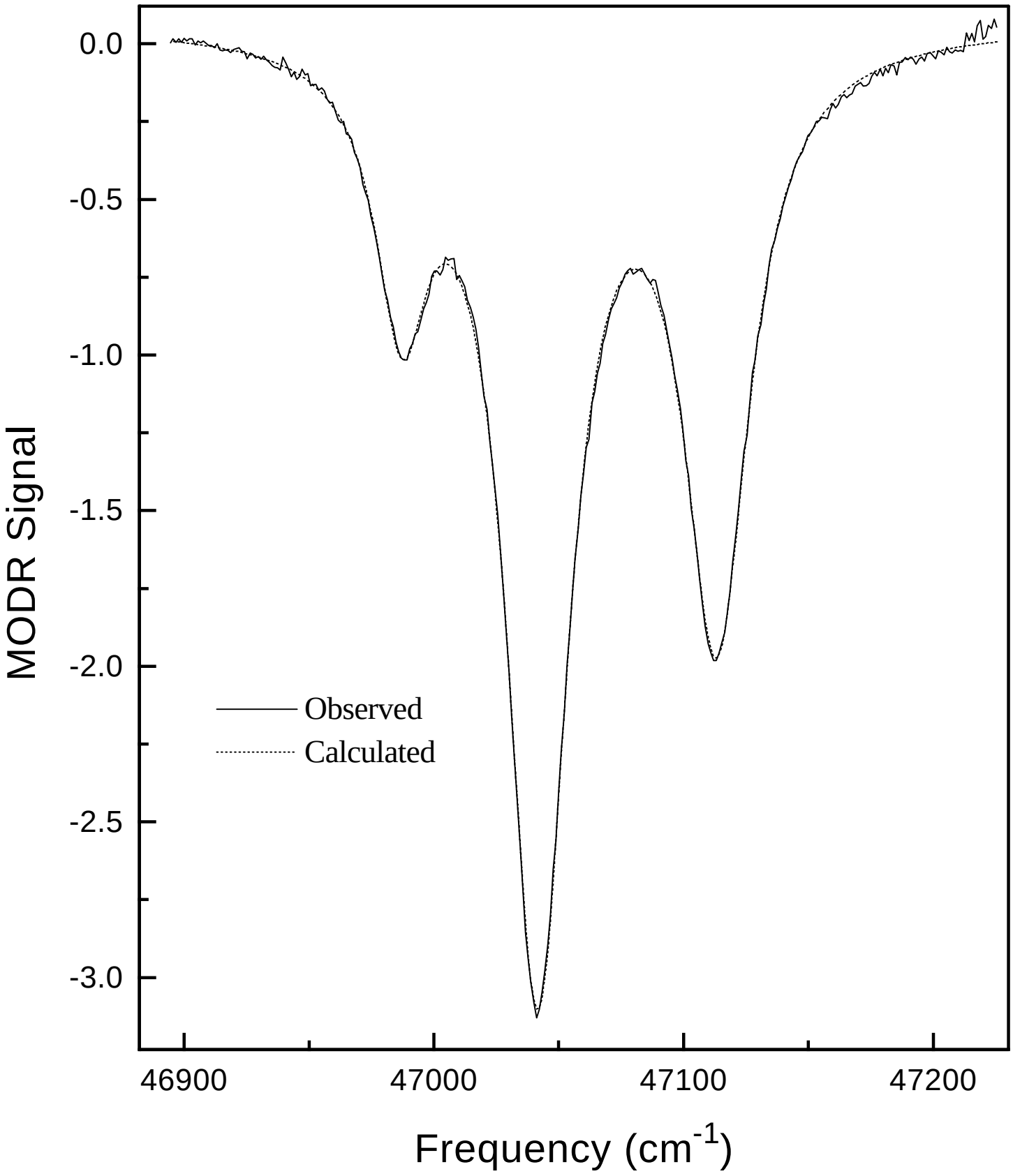
0.0
-0.5
-1.0
-1.5
-2.0
-2.5
-3.0
MODR Signal
Observed
Calculated
46900
47000
47100
47200
Frequency (cm-1)